J|A|C|S ARTICLES

Published on Web 07/01/2009

Lamellar Envelopes of Semiconductor Nanocrystals

Anna Lee, Neil A. Coombs, Ilya Gourevich, Eugenia Kumacheva, and Gregory D. Scholes*

Department of Chemistry, Institute for Optical Sciences and Centre for Quantum Information and Quantum Control, University of Toronto, 80 St. George Street, Toronto, Ontario, M5S 3H6 Canada

Received March 26, 2009; E-mail: gscholes@chem.utoronto.ca

Abstract: We report the solution-phase formation of ordered lamellar nanocrystal (NC) arrays. These semiconductor lamellae exhibit structural integrity and temporal stability, without recourse to chemical cross-linking. They are many micrometers in diameter yet only two or three nanocrystal layers in thickness. We show that these structures can integrate a cargo of water-soluble ions, molecules, metal nanoparticles, or biomolecules. Encapsulation of gold nanoparticles is found to cause photoluminescence enhancement of the host CdSe nanocrystals. These easily prepared nanocrystal "envelopes" promise properties modulated through the integration of a vast array of water-soluble species. Our approach marks a step toward ordered, compartmentalized, NC-based complexes with controlled architectures.

Introduction

Organization of complex suprastructures in nanoscale systems, both natural and synthetic, is of immense interest in many fields of science. Nanoscale building blocks such as polymer molecules, colloidal particles, surfactants, proteins, and liquid crystals can conceptually be viewed as "atoms" or "molecules" that, when assembled, form the basis of new classes of materials.[1−7] Colloidal semiconductor nanocrystals (NCs) are interesting materials to consider as building blocks because of their particular optical and electronic properties that can be tuned by size, shape, and composition.[8−10] The organization of NCs into large arrays is of interest both fundamentally and for practical uses of NCs in "bottom-up" design.

Controlled assembly of NCs has been pursued by, for example, the three layer oversaturation technique for the formation of three-dimensional NC superlattices[11] and by the assembly of free-floating monolayer NC sheets by electrostatic and hydrophobic interactions in conjunction.[12] NC assembly has also been accomplished at liquid/liquid interfaces where reduction of interfacial energy drives the formation of NC monolayers at the spherical surface of micrometer-diameter droplets.[13,14] Some of the most strikingly ordered NC superlattice structures reported to date are formed by controlled evaporation of a NC suspension onto a substrate.[15,16]

Here we report a simple, in solution, procedure that involves controlled addition of a nonsolvent (water) together with sonication to trigger the formation of micrometer-size lamellar sheets of ordered NC arrays. The most striking characteristics of these systems are that, while they are many micrometers in diameter, they are uniformly only two or three NC layers in thickness (∼15 nm), yet they exhibit structural integrity without the need for chemical cross-linking.[17] In addition, the properties of the lamellar structures can be modified by internalizing water-soluble species including ionic salts, metal nanoparticles (NPs), and biomolecular complexes.

Experimental Section

Preparation of QD Lamellar Structures. Trioctylphosphine oxide (TOPO) capped CdSe quantum dots (QDs) were synthesized through an established organometallic approach at high temperature.[18,19] Nanorods were prepared by a method described elsewhere[20] with the exception that a mixture of equimolar amounts (9 mmol) of $Cd(OAc)_2 \cdot 2H_2O$ and $NH_4(OAc)$ was used in the multi-injection step. As-synthesized TOPO capped CdSe QDs or nanorods were precipitated with methanol three times to remove free TOPO and then dissolved in toluene. For optimmized lamellar formation, 10 μL of deionized water (10% v/v) were added into CdSe QDs

(1) Whitesides, G. M.; Boncheva, M. *Proc. Natal. Acad. Sci. U.S.A.* **2002**, *99*, 4769–4774.
(2) Whitesides, G. M.; Grzybowski, B. *Science* **2002**, *295*, 2418–2421.
(3) Antonietti, M.; Goltner, C. *Angew. Chem., Int. Ed. Engl.* **1997**, *36*, 910–928.
(4) Hamley, I. W. *Angew. Chem., Int. Ed.* **2003**, *42*, 1692–1712.
(5) Ozin, G. A. *Adv. Mater.* **1992**, *4*, 612–649.
(6) Philp, D.; Stoddart, J. F. *Angew. Chem., Int. Ed. Engl.* **1996**, *35*, 1155–1196.
(7) Glotzer, S. C.; Solomon, M. J. *Nat. Mater.* **2007**, *6*, 557–562.
(8) Alivisatos, A. P. *Science* **1996**, *271*, 933–937.
(9) Weller, H. *Angew. Chem., Int. Ed. Engl.* **1996**, *35*, 1079–1081.
(10) Scholes, G. D.; Rumbles, G. *Nat. Mater.* **2006**, *5*, 683–696.
(11) Rogach, A. L.; Talapin, D. V.; Shevchenko, E. V.; Kornowski, A.; Haase, M.; Weller, H. *Adv. Func. Mater.* **2002**, *12*, 653–664.
(12) Tang, Z. Y.; Zhang, Z. L.; Wang, Y.; Glotzer, S. C.; Kotov, N. A. *Science* **2006**, *314*, 274–278.
(13) Boker, A.; He, J.; Emrick, T.; Russell, T. P. *Soft Matter* **2007**, *3*, 1231–1248.
(14) Lin, Y.; Skaff, H.; Emrick, T.; Dinsmore, A. D.; Russell, T. P. *Science* **2003**, *299*, 226–229.
(15) Murray, C. B.; Kagan, C. R.; Bawendi, M. G. *Science* **1995**, *270*, 1335–1338.
(16) Shevchenko, E. V.; Talapin, D. V.; Kotov, N. A.; O'Brien, S.; Murray, C. B. *Nature* **2006**, *439*, 55–59.
(17) Lin, Y.; Skaff, H.; Boker, A.; Dinsmore, A. D.; Emrick, T.; Russell, T. P. *J. Am. Chem. Soc.* **2003**, *125*, 12690–12691.
(18) Murray, C. B.; Norris, D. J.; Bawendi, M. G. *J. Am. Chem. Soc.* **1993**, *115*, 8706–8715.
(19) Peng, Z. A.; Peng, X. G. *J. Am. Chem. Soc.* **2001**, *123*, 183–184.
(20) Nair, P. S.; Fritz, K. P.; Scholes, G. D. *Small* **2007**, *3*, 481–487.

10.1021/ja902218q CCC: $40.75

(9.84×10^{-7} mol/L) dissolved in toluene (20% v/v water was used for nanorods). The mixtures were sonicated from 15 to 30 s at 42 kHz. A cloudy, colored suspension formed immediately following sonication. The sample was withdrawn via micropipet for further characterization. For all encapsulation experiments, 10 μL (10% v/v) of water-soluble species ($CoCl_2 \cdot 6H_2O$, 6.09×10^{-2} M; $EuCl_3 \cdot 6H_2O$, 7.39×10^{-2} M; Au NPs ~37.8 nM, and ferritin 53 mg/mL in 0.15 M NaCl) were added as described above for water.

Chracterization of the Structure of Lamellar NC Arrays. For scanning transmission electron microscopy (STEM), a single droplet of solution (~25 μL) was applied to 400 mesh or 200 mesh carbon coated copper TEM grids and also to 1000 mesh uncoated TEM grids for the preparation shown in Figure 2C. Images in both bright field and high angle annular dark field (HAADF) were recorded using the Hitachi HD-2000 dedicated STEM operating at 200 kV. For the cross-sectional analysis, samples were first prepared on carbon coated indexed TEM grids. STEM was used to identify the locations of individual lamellae. Subsequently, the indexed grids were coated with ~10 nm of carbon using an Emitech high vacuum carbon coater. Grids were then coated with a 20−30 nm layer of Au using a Denton Desk II sputter coater. The indexed grids were then embedded in epoxy resin, and 30 nm cross sections were prepared using a Leica Ultramicrotome (Figure S6). For solution state imaging of lamellae, samples (~15 μL) were injected into Quantomix WETSEM capsules and backscattered electron images recorded using a Hitachi S-3400 SEM operating at 20 kV and with the Hitachi TM-1000 table top variable pressure SEM operating at 15 kV. Energy dispersive X-ray spectroscopy (EDS) in both SEM and STEM was carried out using an Oxford Instruments INCA system. STEM EDS analysis of cross sections was performed at −120 °C to minimize electron beam damage and contamination during X-ray acquisition. Simultaneous TEM and SEM were recorded using a Hitachi S-5200 field emission SEM equipped with a transmitted electron detector. Liquid state confocal fluorescence microscopy was carried out using a Leica TCP SP2 upright confocal microscope with a ×63 1.4 oil immersion lens. The 364 nm line on an Innova 90C Argon ion laser was used for excitation with the signal collected over a range from 550 to 600 nm. Fluorescence intensity studies were carried out by recording a series of sequential fluorescence images in a range from 500 to 700 at 5 nm intervals. Again, the 364 nm line of an Innova 90C Argon ion laser was used for excitation (Figure S13). For the analysis of dye (FITC 100 ng/mL) incorporation into the lamellae, fluorescent images were obtained using a Leica TCS SP2 confocal microscope with a ×63 1.4 oil immersion lens. Both FITC and QD lamellae were excited using the 488 nm line of an argon ion laser. FITC emission was collected in the range 490−530 nm Ch1 (green). CdSe QD emission was collected in the range 550−600 nm Ch2 (yellow). Selected area electron diffraction (SAED) patterns of CdSe QDs and nanorods and their lamellar structures were recorded using an FEI Technai 20 operating at 200 kV (Figure S14). Subsequent analysis of polycrystalline ring patterns was carried out using the Process Diffraction software package.[21]

Results and Discussion

The CdSe NCs (mean diameter 4.0 nm) and CdSe bullet-shaped nanorods[20] (mean length 19 nm, width 11 nm) (Figure S1) were capped with trioctylphosphine oxide (TOPO) whose hydrophobic tails stabilize nanoparticles in nonpolar solvents. Addition of a controlled amount of water to a suspension of NCs in toluene, followed by sonication, led to the formation of pancake-shaped lamellae. After 20 s sonication we observed three distinct phases: the majority phase consisting of large disk-like QD lamellae (mean diameter 20 μm), smaller droplets coated with QDs,[14] and larger disordered aggregates (Figure 1A). At shorter (less than 10 s) sonication times two distinct phases were observed: QD-coated droplet-like structures (the major phase) (Figure 1B) and the QD lamellae. Given the inherent shallow depth of focus of confocal fluorescence microscopy, our observations clearly differentiated the flat, pancake-like morphologies from the surrounding droplets which consistently exhibited the strongest fluorescence intensity at their periphery.

To confirm the liquid state fluorescence microscopy results, we carried out "wet-cell" scanning electron microscopy (SEM) in which solution-state samples (~15 μL), contained within a sealed chamber, were viewed through a window transparent to electrons. We employed backscattered electron (BSE) imaging. BSE images, whose signal is atomic number-dependent, clearly showed CdSe NC lamellae, droplets, and disordered aggregates (Figure 1C and 1D). Energy dispersive X-ray spectroscopy (EDS) of a single lamellar structure, in solution, confirmed the presence of Cd and Se (Figure S2). Furthermore, a BSE video was recorded showing the existence of the lamellae floating in solution (Movie S1). In addition to its atomic number dependence, BSE signals are also sensitive to sample thickness. Image intensity profiling across a single lamella revealed a uniform, flat, greyscale value for the structure (Figure 1E), which was consistent with those observed in confocal fluorescence microscopy. The lamellae were temporally stable: solution samples imaged 3 months after original self-assembly experiments contained intact lamellae (Figure S3). The generality of the approach was supported by the formation of qualitatively similar lamellar structures using PbS NCs capped with oleic acid and CdTe NCs capped with tetradecylphosphonic acid (Figure S4).

The formation of NC lamellae was dependent on the sonication time and the concentration of water. The effect of sonication time was examined by varying it from 5 to 180 s at a fixed sonication frequency (42 kHz ± 6%) and energy (70 W). For times shorter than 10 s, assembly of NCs was dominated by the formation of micrometer-size droplets, similar to those produced by mechanical agitation,[14] with the exception that the average droplet size in our work was measurably smaller. At sonication times in the range 15−30 s, lamellae were the predominant structures. The transition from droplets to lamellae resembled the formation of intermediate disk-like pancake structures induced by sonication of liposomes.[22] At longer sonication times, greater than 150 s, we observed small, dense spheroidal structures and disordered precipitates of NCs.

With respect to water concentration, we observed that at 5 vol % water and below, small, poorly ordered disk-like structures formed, which had no structural integrity. Under these conditions, the absence of lamellae could be statistical: although lamellae might form, they were present in too small numbers to be readily detected by microscopy. In contrast, addition of greater than 20 vol % water produced disordered aggregates and dense spheroidal NC structures. Under these conditions, it is likely that at a constant concentration of NCs, the number of NCs per unit area of toluene/water interface decreases, resulting in incomplete interfacial coverage and structural instability of the lamellae. As a consequence of these observations, we optimized lamellar formation by the addition of 10 vol % of H_2O to the solution of NCs.

Scanning transmission electron microscopy (STEM) images of pancake-shaped lamellae (Figure S5A for NCs and S5B for nanorods) confirmed that the self-assembled structures were preserved during the drying process. High magnification views

(21) Labar, J. L. *Ultramicroscopy* **2005**, *103*, 237–249.

(22) Lasic, D. D. *Liposomes from physics to applications*; Elsevier: 1993.

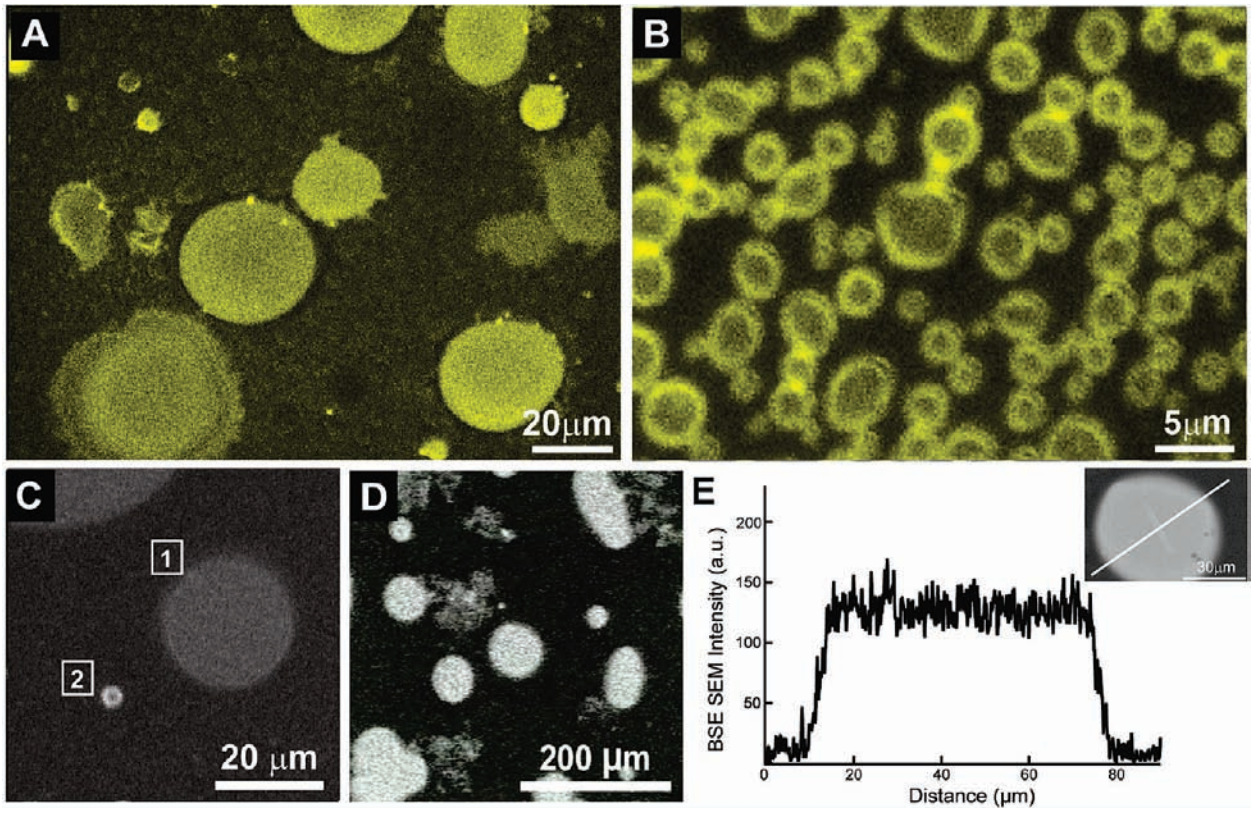

Figure 1. (A) Liquid state confocal fluorescence microscopy image of CdSe NC lamellae formed by the addition of 10% (v/v) water with subsequent 20 s sonication. (B) Confocal image of the same preparation as (A) at less than 10 s sonication time. Confocal images were recorded using an oil immersion lens (excitation at 364 nm, detection 550 to 600 nm). (C) Solution state "Wet cell" BSE image showing the existence of large lamellar structures (see 1) in solution along with small droplets (see 2) whose greatest signal exists at its periphery. (D) Solution state "Wet cell" BSE image overview of large lamellae along with disordered aggregates. (E) Image intensity profiling of a lamella (inset) showing uniform intensity consistent with a disk- or sheetlike structure.

indicated a significant degree of order within the lamellar structures for both NCs (Figure 2A) and nanorods (Figure 2B). Furthermore, NC overlap, indicated by apparent linear features in images of NC lamellae (Figure 2A inset 1) and by the fine lines subdividing individual NCs in images of nanorod lamellae (Figure 2B inset 1), suggested the presence of multiple layers of NCs. Fourier transform analyses for both systems indicated a clear tendency to hexagonal symmetry in the NC packing perpendicular to the plane of the lamellae (Figure 2A and 2B, inset 2). The arrays exhibited a high degree of order, similar to that achieved using controlled solvent evaporation.[15,16,23]

The NC lamellae featured structural integrity: when mounted on uncoated TEM grids they spanned the voids in the grid structure and withstood imaging by the high-energy electron beam without deformation (Figure 2C). Given that these lamellae appear to be only a few NC layers in thickness, it was surprising that they were able to span distances 3 orders of magnitude larger, up to 15 μm, without support. Folds and tears observed in STEM images of individual NC lamellae served as additional indicators of their structural integrity (Figure 2D). The structural integrity of the NC lamellae resembled elastic membranes formed by noncross-linked monolayers of Au NPs, which spanned voids with dimensions of up to 1 μm.[24]

The results of confocal fluorescence microscopy experiments (Figure 1A) and wet cell SEM (Figure 1C and 1D) in combination with the observed NC overlap in the lamellae of spherical nanoparticles and nanorods (Figure 2A and 2B) suggested the presence of a sheet-like structure with more than one layer of NCs. To elucidate the cross-sectional structure of the lamellae, they were deposited on indexed TEM grids, stabilized by the deposition of an ~10-nm-thick carbon coating and a 20−30-nm-thick gold layer and microtomed to ~30-nm-thick sections. The STEM images of both NC and nanorod lamellae showed well-ordered bi- and trilayers (Figure 2E and 2F, Figures S6 and S7, respectively). EDS line profiling across a trilayer structure of NCs confirmed the presence of Cd, Se, and P (Figure S8). The P signal indicated that TOPO was present within the structure.

To reconcile the plan view and the cross-sectional structure of the NC lamellae (Figure 2A and Figure 2E, F, respectively) we propose the following interpretation of our results. For a NC bilayer in plan view, we observe projections of individual NCs in a hexagonal arrangement that are surrounded by linear structures that follow the same symmetry (Figure 2A). These discrete, "individual" NC projections correspond to two NCs with vertical alignment with AA-type layer stacking, whereas the linear structures are likely the result of AB-type layer stacking. Consistent with this observation, cross-sectional images (Figure 2E and F) show both regions of discrete single NC alignment along with extensive regions of NC overlap. While it is also possible that coverage in the second layer is incomplete, and NCs lie at the 2-fold sites, instead of the normal 3-fold

(23) Talapin, D. V.; Shevchenko, E. V.; Murray, C. B.; Titov, A. V.; Kral, P. *Nano Lett.* **2007**, *7*, 1213–1219.
(24) Mueggenburg, K. E.; Lin, X. M.; Goldsmith, R. H.; Jaeger, H. M. *Nat. Mater.* **2007**, *6*, 656–660.

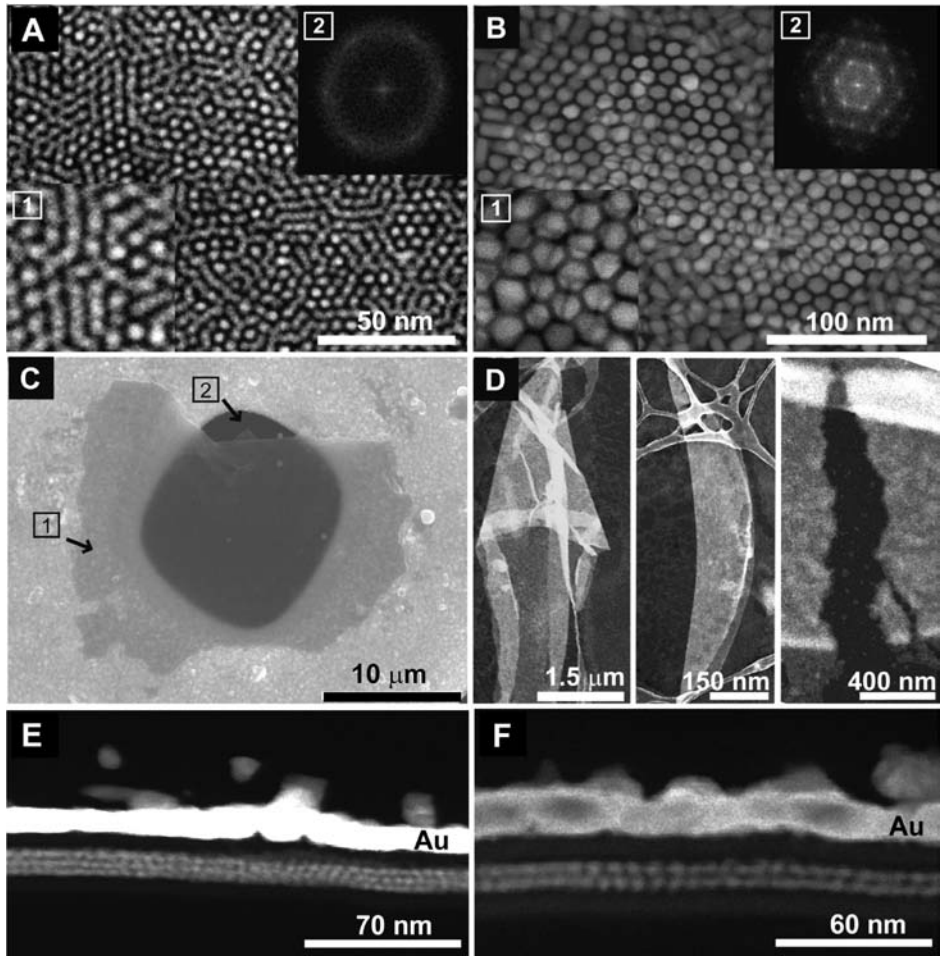

Figure 2. (A) STEM image of a NC lamella. Inset 1 shows NC ovelap indicated by linear structures. Fourier transform (inset 2) indicates hexagonal symmetry. (B) STEM image of a nanorod lamella inset 1 shows nanorod ovelap indicated by fine lines subdividing individual NCs. A region of ordered hexagonal packing is confirmed by Fourier transform (inset 2). (C) SEM image of a lamella (see 1) mounted on an uncoated Cu TEM grid. The lamella (~15 nm thick) spans the dark void (~15 μm) (see 2) in the grid without support. (D) Examples of folds and tears present in lamellae indicating their structural integrity. (E and F) Cross-sectional STEM images of NC tri- and bilayers. For all cross sections, the thickness is ~30 nm. The capping Au overlayer is used as a location marker.

sites for hard sphere stacking, the STEM images of lamellae cross sections show extensive areas of continuous multilayers of NCs.

The NC center-to-center spacing of ~6.5 nm in the plane of the lamellae was similar to that observed for control samples (CdSe NCs deposited from toluene solution onto carbon coated TEM grids and assembled via evaporation) (Figure S1). However, the NC-to-NC spacing between the layers was only ca. 4.5 nm (Figure 2E and 2F). We conjecture that water may play a role in the preferential vertical compression between NC layers by inducing asymmetries in either ligand distribution or conformation, driven by hydrophobic effects. In either case, the reduction in interlayer distance between adjacent NCs is likely to increase their dipole interactions,[12,23] which may be an important factor in the structural integrity of these lamellae (the ground state dipole in the crystal is ~100 D).[25]

We note that even if dipole−dipole interactions and hydrophobic forces between the QDs are sufficient to stabilize the lamellae, the question remains: what is the driving force for their formation? Assembly of QDs at the surface of aqueous droplets, driven by the reduction of interfacial energy,[14,17]occurred at short (<10 s) sonication times. As such, these droplets likely served as precursors to the lamellar structures formed at longer sonication times (15−30 s). We suggest that exposure to ultrasound plays a key role by generating a mechanical force in the system. Acoustic cavitation, a major effect of low-frequency sonication, induces high magnitude shear around oscillating bubbles.[26,27] It has been established that shear forces tend to stretch and elongate the emulsion droplets (while surface tension forces try to counterbalance this effect).[28] We conjecture that, with sufficient elongation, the opposing walls of a droplet are brought into close enough proximity that dipole−dipole and hydrophobic forces acting between the QDs stabilize the resulting 2D lamellar structure. From a more general perspective, at the molecular and supramolecular level, acoustic cavitation effects have just begun to be recognized as a new route to the production of novel architectures that cannot be obtained otherwise.[29−32]

(25) Shim, M.; Guyot-Sionnest, P. *J. Chem. Phys.* **1999**, *111*, 6955–6964.
(26) Elder, S. A. *J. Acoust. Soc. Am.* **1959**, *31*, 54–64.
(27) Richardson, E. S.; Pitt, W. G.; Woodbury, D. J. *Biophys. J.* **2007**, *93*, 4100–4107.
(28) Cristini, V.; Guido, S.; Alfani, A.; Blawzdziewicz, J.; Loewenberg, M. *J. Rheol.* **2003**, *47*, 1283–1298.
(29) Bardelang, D. *Soft Matter* **2009**, *5*, 1969.
(30) Paulusse, J. M. J.; Sijbesma, R. P. *Angew. Chem., Int. Ed.* **2006**, *45*, 2334–2337.

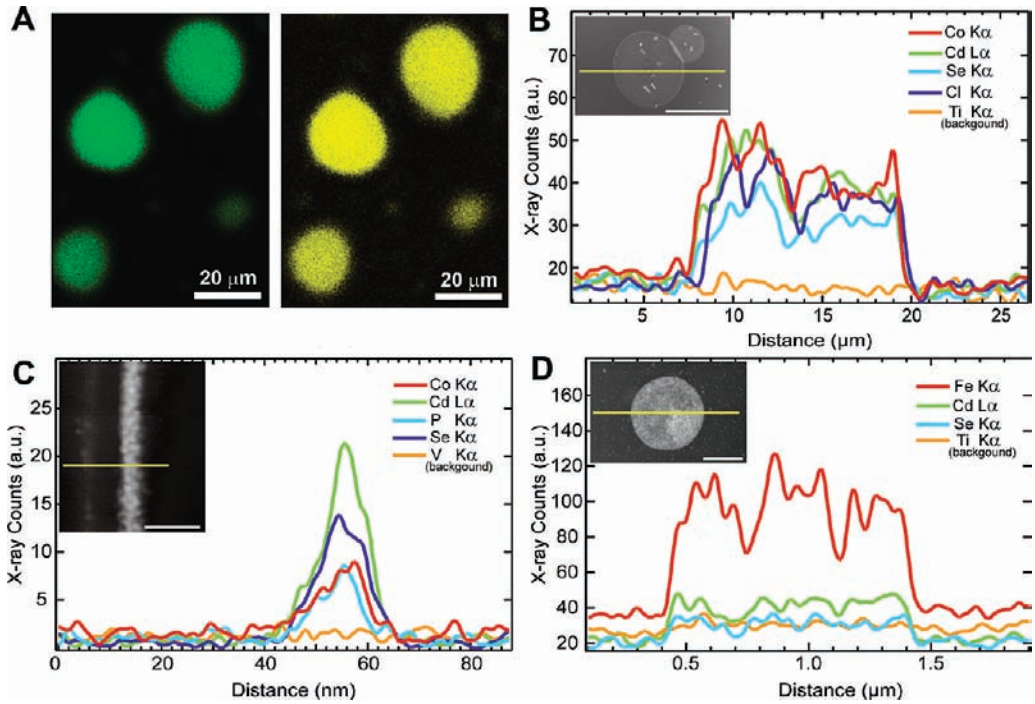

Figure 3. (A) Liquid state confocal fluorescence microscopy images of NC lamellae formed in the presence of the water-soluble dye fluorescein isothiocyanate (FITC), water 10% (v/v). Both FITC and NCs were excited using the 488 nm line of an argon ion laser. Note the coincidence between FITC (green) (collection range 490−530 nm) and NCs (yellow) (collection range 550−600 nm) indicating that the water-soluble dye is associated with the lamellar structure. (B) Energy dispersive X-ray spectroscopic (EDS) line scans for $CoCl_2 \cdot 6H_2O$ incroporated into CdSe lamellae. The inset shows an HAADF STEM image with the line scan (yellow line) across the lamellar structure (scale bar: 10 μm). (C) EDS line scan of a cross-sectioned (~70 nm thick) Co incorporated NC lamellar bilayer showing the presnce of Co within the structure. The inset shows corresponding HAADF STEM image (scale bar: 35 nm). (D) EDS data for ferritin incorporated into the lamellae. The inset shows a corresponding HAADF STEM image (scale bar: 500 nm). Note: Ti Kα or V Kα lines were used as backgrounds since they have no spectral overlap with the elements of interest.

If water, in the course of formation of the lamellae, is confined between the NC sheets, then not only is this important in understanding the structure of the lamellae but it also offers an opportunity to incorporate, in the "envelopes", a wide variety of water-soluble species. To test the validity of this hypothesis, we prepared NC lamellae in the presence of the water-soluble dye, fluorescein isothiocyanate (FITC). Liquid state confocal fluorescence microscopy showed matching localization of photoluminescence (PL) from FITC and CdSe in the NC lamellae (Figure 3A). To build from this observation and exploit its implications, we have incorporated a number of water-soluble ionic, molecular, nanocrystalline and biomolecular species into CdSe NC lamellae.

EDS line scans across individual lamellae showed that cobalt (Figure 3B) and europium (Figure S9), introduced as salts in H_2O (10% v/v), were strongly partitioned within the NC lamellae. Furthermore, EDS line scans of cross sections of lamellae prepared with Co salts confirmed the presence of Co within the lamellar structure (Figure 3C).

The incorporation of larger molecules in the lamellae interior was demonstrated for water-soluble tris(2,2′-bipyridyl)ruthenium(II) (Figure S10) and the biological macromolecule, ferritin. Ferritin is an iron-storage protein consisting of a protein shell surrounding a nanocrystalline iron complex core[33] (Figure S11). EDS line scans showed the presence of Fe and by implication ferritin (Figure 3D). The very strong Fe signal is an indicator of the high loading potential of NC lamellae.

As a specific example of the encapsulation of water-soluble species, citrate-capped Au spheroidal nanoparticles (NPs) with a mean diameter of 10 nm were incorporated into CdSe NC lamellae. As with the other water-soluble species studied, the Au NPs were found exclusively within the lamellae (Figure 4A). EDS mapping showed the uniform distribution of Cd and Se and well dispersed discrete Au signals consistent with the presence of Au NPs (Figure S12). To confirm that the Au NPs were internalized, two approaches were taken. First, cross-sectional STEM imaging (Figure 4B) showed the presence of Au NPs within the lamellar structure. Second, simultaneous high resolution surface (SEM) and transmitted (TEM) images of the same lamellar region were recorded. These results showed that the Au NPs were encapsulated (Figure 4C and 4D), in clear contrast to a control experiment (Figure 4E) where Au NPs were added after lamellar formation.

When semiconductor NCs are coupled with metal NPs, plasmon-exciton interactions result in either enhancement or quenching of NC photoluminescence.[34,35] Enhancement of emission occurs due to the plasmon-induced field enhancement effect, whereas quenching of NC emission is due to energy

(31) Bardelang, D.; Camerel, F.; Margeson, J. C.; Leek, D. M.; Schmutz, M.; Zaman, M. B.; Yu, K.; Soldatov, D. V.; Ziessel, R.; Ratcliffe, C. I.; Ripmeester, J. A. *J. Am. Chem. Soc.* **2008**, *130*, 3313.
(32) Hickenboth, C. R.; Moore, J. S.; White, S. R.; Sottos, N. R.; Baudry, J.; Wilson, S. R. *Nature* **2007**, *446*, 423–427.
(33) Lawson, D. M.; Artymiuk, P. J.; Yewdall, S. J.; Smith, J. M. A.; Livingstone, J. C.; Treffry, A.; Luzzago, A.; Levi, S.; Arosio, P.; Cesareni, G.; Thomas, C. D.; Shaw, W. V.; Harrison, P. M. *Nature* **1991**, *349*, 541–544.
(34) Shimizu, K. T.; Woo, W. K.; Fisher, B. R.; Eisler, H. J.; Bawendi, M. G. *Phys. Rev. Lett.* **2002**, *89*, 117401.
(35) Hosoki, K.; Tayagaki, T.; Yamamoto, S.; Matsuda, K.; Kanemitsu, Y. *Phys. Rev. Lett.* **2008**, *100*, 207404.

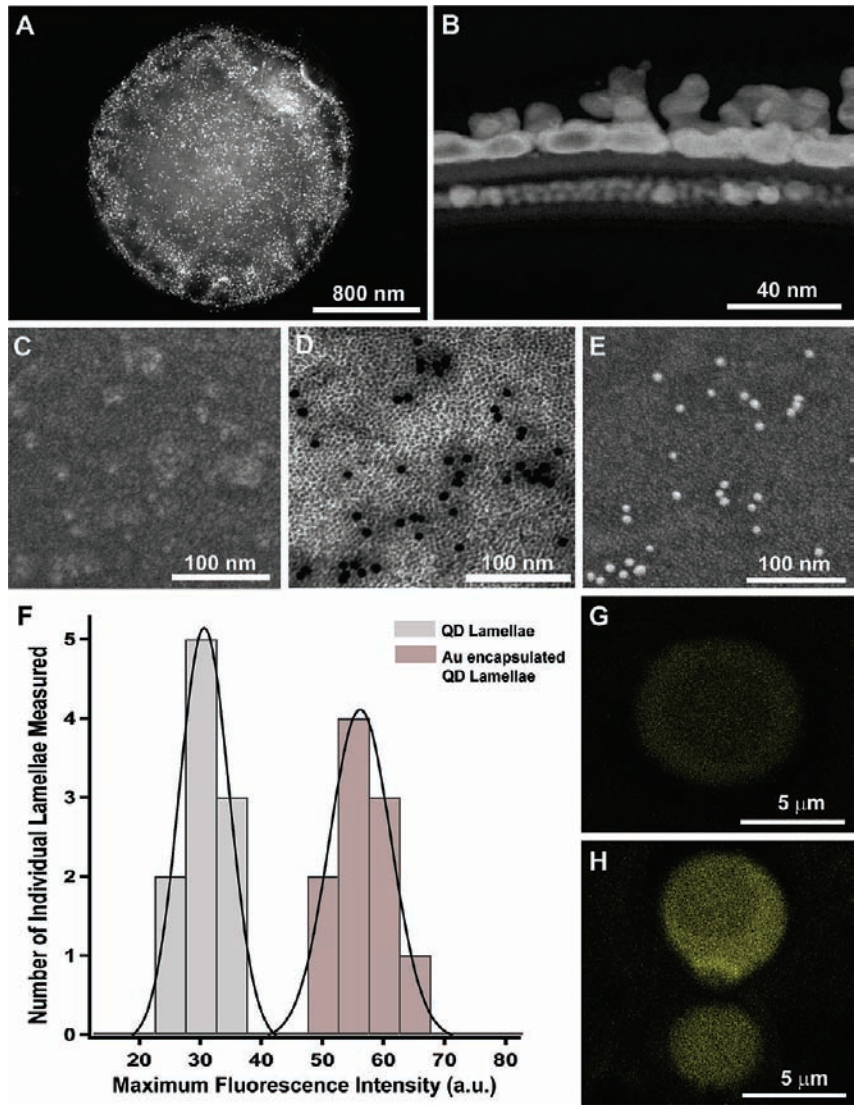

Figure 4. (A) Incorporation of Au NPs into CdSe NC lamellae. In the HAADF STEM image shown, the bright "dots" are individual Au NPs. (B) Cross-sectional (~30 nm thickness) STEM image confirming the encapsulation of Au NPs inside the NC bilayer (as previously, an evaporated Au layer, upper portion of the image, is used as a marker). (C and D) Simultaneously recorded SEM and TEM images, respectively, confirming encapsualtion of Au NPs within the NC lamellae. (E) SEM image of control sample with Au NPs added after the NC lamellae formation. (F) Histogram showing 10 maximum photoluminescense intensity measurements for both NC lamellae and Au encapsulated NC lamellae. (G and H) Representative fluorescence confocal microscope images of CdSe NC lamellae and Au encapsulated NC lamellae, respectively.

transfer from NC to metal NPs.[36,37] This plasmon-exciton coupling interaction is of both theoretical and practical interest in the areas of light emitting devices, nanoscale lasing, and solar cells etc. To study the effects of encapsulation of Au NPs on the luminescence of CdSe lamellae, photoluminescence (PL) spectra were measured using confocal fluorescence microscopy for 10 randomly selected lamellae compartmentalizing Au NPs. Lamellae formed by CdSe NCs only were used in control experiments. Representative confocal fluoresence microscopy images of control and Au NP encapsulated CdSe lamellae are presented in Figure 4G and 4H, respectively. To compare the relative PL yield from each of these structures, we plotted two histograms of the integrated PL intensity. Figure 4F shows a near doubling of the PL intensity for the Au encapsulated lamellae, compared to the control sample. This PL enhancement occurred due to electronic interactions between the Au NPs and the CdSe NCs in the "hybrid" lamellae.[38] This interaction could result from plasmonic enhancement of the NC radiative rate,[39] or NC PL could be sensitized by resonance energy transfer from Au NPs.[40] A weak blue shift of PL maximum (582 to 574 nm) similar to that shown in previous studies was observed.[41,42] Analogous to the argument of Lee et al.,[41] the blue shift may arise due to decreased exciton diffusion length as a result of the increased radiative decay rate caused by exciton−plasmon interactions. Optimization for luminescence enhancement of the lamellar structure will require control of experimental param-

(36) Govorov, A. O.; Bryant, G. W.; Zhang, W.; Skeini, T.; Lee, J.; Kotov, N. A.; Slocik, J. M.; Naik, R. R. *Nano Lett.* **2006**, *6*, 984–994.
(37) Govorov, A. O.; Lee, J.; Kotov, N. A. *Phys. Rev. B* **2007**, *76*, 125308.
(38) Barnes, W. L. *J. Mod. Opt.* **1998**, *45*, 661–699.
(39) Chance, R. R.; Prock, A.; Sibey, R. *Adv. Chem. Phys.* **1978**, *37*, 1.
(40) Saini, S.; Shenoy, V. B.; Bagchi, B. *J. Phys. Chem. C* **2008**, *112*, 6299–6306.
(41) Lee, J.; Govorov, A. O.; Dulka, J.; Kotov, N. A. *Nano Lett.* **2004**, *4*, 2323–2330.
(42) Hsieh, Y. P.; Liang, C. T.; Chen, Y. F.; Lai, C. W.; Chou, P. T. Nanotech. 2007, *18*,

eters, e.g., the type of encapsulated NPs, choice of QDs, their concentrations, shape, dimensions, and variation of interparticle distances.[36,37,43−45]

Conclusions

In summary, we have demonstrated a facile procedure for producing solution state, micrometer-large bi- and trilayer lamellae formed by semiconductor nanoparticles. These structures exhibited strength and NC order and showed the ability to encapsulate a variety of water-soluble species. The capability to tune the optical properties of the NC lamellae was demonstrated by enhancing PL intensity via the incorporation of Au NPs. We speculate that these ions or molecular complexes may be useful in photoelectrochemical processes, e.g., in forming redox couples in an ordered, nanoparticle solar cell.[46−48] More fundamentally, these structures mark a step toward ordered, compartmentalized, NC-based synthetic complexes whose properties can be modulated by the cargo they carry.

Acknowledgment. We thank D. Hoyle (Hitachi High Technologies Canada) for his assistance with BSE "wet cell" imaging, H. Zhong for providing CdTe NCs, and A. Zabet-Khosousi and A. Dhirani for kindly providing a sample of gold nanoparticles. The Natural Sciences and Engineering Research Council of Canada is gratefully acknowledged for support of this research. G.D.S. acknowledges the support of an EWR Steacie Memorial Fellowship. E.K. thanks Canada Research Chair for support.

Supporting Information Available: Additional figures and a movie. This material is available free of charge via the Internet at http://pubs.acs.org.

JA902218Q

(43) Kulakovich, O.; Strekal, N.; Yaroshevich, A.; Maskevich, S.; Gaponenko, S.; Nabiev, I.; Woggon, U.; Artemyev, M. *Nano Lett.* **2002**, *2*, 1449–1452.
(44) Chen, C. W.; Wang, C. H.; Wei, C. M.; Chen, Y. F. *Appl. Phys. Lett.* **2009**, *94*, 071906.
(45) Pompa, P. P.; Martiradonna, L.; Della Torre, A.; Della Sala, F.; Manna, L.; De Vittorio, M.; Calabi, F.; Cingolani, R.; Rinaldi, R. *Nat. Nanotech.* **2006**, *1*, 126–130.
(46) Gratzel, M. *Nature* **2001**, *414*, 338–344.
(47) Hagfeldt, A.; Gratzel, M. *Chem. Rev.* **1995**, *95*, 49–68.
(48) Kamat, P. V. *J. Phys. Chem. C* **2008**, *112*, 18737–18753.